Nlcam modulates midline convergence during anterior neural plate morphogenesis

Katherine E. Brown [a,c], Philipp J. Keller [a,b], Mirana Ramialison [a], Martina Rembold [a,1], Ernst H.K. Stelzer [b], Felix Loosli [a,d], Joachim Wittbrodt [a,c,d,*]

[a] Developmental Biology, European Molecular Biology Laboratory, Meyerhofstrasse 1, 69117 Heidelberg, Germany
[b] Cell Biology and Biophysics Units, European Molecular Biology Laboratory, Meyerhofstrasse 1, 69117 Heidelberg, Germany
[c] University of Heidelberg, HIZ, INF 230, 69120 Heidelberg, Germany
[d] Karlsruhe Institute of Technology, KIT, Campus North, ITG, Postfach 3640, 76021 Karlsruhe, Germany

ARTICLE INFO

ABSTRACT

During development, different cell types must undergo distinct morphogenetic programs so that tissues develop the right dimensions in the appropriate place. In early eye morphogenesis, retinal progenitor cells (RPCs) move first towards the midline, before turning around to migrate out into the evaginating optic vesicles. Neighbouring forebrain cells, however, converge rapidly and then remain at the midline. These differential behaviours are regulated by the transcription factor Rx3. Here, we identify a downstream target of Rx3, the Ig-domain protein Nlcam, and characterise its role in regulating cell migration during the initial phase of optic vesicle morphogenesis. Through sophisticated live imaging and comprehensive cell tracking experiments in zebrafish, we show that ectopic expression of Nlcam in RPCs, as is observed in Rx3 mutants, causes enhanced convergence of these cells. Expression levels of Nlcam therefore regulate the migratory properties of RPCs. Our results provide evidence that the two phases of optic vesicle morphogenesis: slowed convergence and outward-directed migration, are under different genetic control. We propose that Nlcam forms part of the guidance machinery directing rapid midline migration of forebrain precursors, where it is normally expressed, and that its ectopic expression upon loss of Rx3 imparts these migratory characteristics upon RPCs.

© 2010 Elsevier Inc. All rights reserved.

Introduction

Shaping the developing embryo requires the orchestration of complex morphogenetic events, ranging from cell shape changes and folding of epithelia, to cell rearrangements and migration. Together, these determine the shape, size and position of body parts and organs. These cell movements must be very tightly coordinated in space and time, and this involves the dynamic transcriptional regulation of effector genes that control cell shape, polarity, adhesion and migration.

Cellular adhesion is central to many aspects of morphogenesis. Cell shape change, rearrangement and migration all depend critically on linking the cytoskeleton of a cell to its external substrate–either another cell or the extracellular matrix (ECM)–and this is achieved primarily by adhesion molecules. There are several major families of cell adhesion molecules (CAMs), the most prevalent being cadherins (Halbleib and Nelson, 2006; Tepass et al., 2000), integrins (Bokel and

Brown, 2002; Geiger et al., 2001) and members of the immunoglobulin (Ig)-domain superfamily (Rougon and Hobert, 2003). Dynamic modulation of the expression levels and subcellular localisation of these various factors is crucial to allow morphogenetic processes to occur.

The vertebrate eye provides an attractive model for the study of morphogenesis. After specification of the eye field within the neural plate, the tissue undergoes a series of complex morphogenetic events, forming the bilateral optic cups (reviewed in (Adler and Canto-Soler, 2007; Chow and Lang, 2001). The transparent teleost embryos provide a particularly amenable paradigm for analysis of these processes, and detailed descriptions of retinal morphogenesis are available (Li et al., 2000; Schmitt and Dowling, 1994). However, the underlying cellular mechanisms have only recently begun to be investigated (Cavodeassi et al., 2005; England et al., 2006; Rembold et al., 2006b). In teleosts, where the morphogenesis has been most extensively studied, the eye field originates as a contiguous group of cells, flanked by telencephalic cells anteriorly and laterally, and diencephalic precursors to the posterior (Woo and Fraser, 1995). The initial specification of the eye field, regulated by transcription factors such as Six3 and Pax6, requires the sorting out of retinal vs. non-retinal cells—a process directed by Eph-Ephrin mediated cell–cell adhesion (Cavodeassi et al., 2005; Moore et al., 2004). Subsequent formation of the optic vesicles is a two-step process,

beginning while cells of the neural plate are still converging to the midline. Firstly, RPCs converge more slowly than the surrounding forebrain cells, creating a wider domain from which the optic vesicles will emerge. Subsequently, individual outward-directed migration of RPCs drives the splitting of the eye field and vesicle evagination. Concomitant to these RPC movements, the forebrain takes shape: lateral telencephalic cells converge rapidly towards the midline and diencephalic cells move anteriorly, filling the gap created by the splitting retinal field (England et al., 2006; Rembold et al., 2006b).

The Rx transcription factors play central roles in eye development. In *Xenopus*, fish and mouse, disruption of Rx gene function leads to small or absent eyes (Andreazzoli et al., 1999; Kennedy et al., 2004; Loosli et al., 2003, 2001; Mathers et al., 1997). Teleosts have three Rx genes, of which Rx3 is expressed earliest in the presumptive eye field. In both zebrafish and medaka, null mutants for *rx3* have no eyes. RPCs are specified, but fail to undergo morphogenesis and remain trapped within the forebrain (Loosli et al., 2003; Stigloher et al., 2006; Winkler et al., 2000). 4D imaging analysis has revealed the cellular basis of these morphogenetic defects in the medaka *eyeless* mutant (Rembold et al., 2006b): the mutant retinal cells converge fully towards the midline, and fail to migrate outwards, instead forming an epithelialised neural keel-like structure, similar to the surrounding forebrain cells. Rx3 thus influences both steps of optic vesicle morphogenesis, convergence and evagination.

The functions of Rx1 and Rx2 are less clear; in zebrafish, their expression is dependent upon Rx3 (Loosli et al., 2003), and over-expression of either can induce retinal cell fate (Chuang and Raymond, 2001). However, morpholinos directed against either paralog (or both in combination) does not give an early morphogenetic phenotype (Rojas-Munoz et al., 2005). The degree of redundancy between these three paralogous genes, however, remains to be fully determined. In *Xenopus*, where there are two Rx paralogs, Rx1 has been shown to be important for RPC proliferation, and also directs their migration (Kenyon et al., 2001; Zaghloul and Moody, 2007). In mammals, despite the differences in how morphogenesis occurs (via an outpocketing of the neural epithelium, rather than by individual cell migration), the function of Rx in directing retinal fate and morphogenesis is conserved (Mathers et al., 1997; Medina-Martinez et al., 2009). This conservation is underscored by the fact that mutations in human Rx have been associated with anopthalmia (Voronina et al., 2004).

To date, few targets of Rx genes have been postulated. Manipulation of Rx levels affects the expression patterns of various transcription factors, neurogenic genes and cell cycle regulators (Andreazzoli et al., 1999, 2003; Kennedy et al., 2004; Loosli et al., 2003, 2001; Winkler et al., 2000; Zhang et al., 2000). However, it remains unclear whether any of these factors are direct transcriptional targets of Rx. Moreover, since none of these factors are morphogenetic effectors, they cannot account for the morphological defects of Rx mutants.

In the case of Rx3, the downstream targets, either direct or indirect, should include factors that influence cell migration. Among these are likely to be adhesion molecules, whose differential expression in wild-type (wt) and *rx3⁻* embryos may help to explain the altered behaviour of mutant cells. Here, we identify one such factor: the Ig-domain CAM Nlcam (Mann et al., 2006), which shows elevated expression in the eye field of zebrafish *rx3/chk* mutants. Ectopic over-expression of Nlcam causes a small-eye phenotype, mimicking the *chk* mutant. Through live imaging and cell tracking experiments, we demonstrate that Nlcam modulates the migration of RPCs during the initial phase of midline convergence. Consistent with this, loss of *nlcam* function leads to delayed convergence of lateral forebrain cells. Our results provide the first link between Rx3 and the downstream cellular machinery responsible for controlling the differential migratory behaviour of forebrain and eye cells.

Materials and methods

Fish husbandry

Zebrafish stocks were maintained at 26 °C, and embryos raised at 28 °C. WIK/AB was used as a wt line. Rx3∷GFP transgenic fish were obtained by injecting pBS-ISceI OlRx3∷GFP (Rembold et al., 2006b) into wt embryos. Progeny with strong, eye-specific GFP expression were selected and the line maintained. The *chk^{s399}* line (Loosli et al., 2003) was used.

Cloning

The *nlcam* cDNA (coding region plus partial 5′ and 3′ UTRs) was amplified by RT-PCR from wt cDNA, using the following primers:

Nlcam-F: AATTTACTGACGTACGCAAC
Nlcam-R: ACAGCTTCTGACTCCATTTT

The resulting 1.9 kilobase pairs (kb) product was cloned into pCS2 for mRNA synthesis. The nlcam-GFP fusion was generated by PCR-cloning the *nlcam* coding region (minus the stop codon) into pEGFP-N1 (Clontech). The fusion was subcloned into pCS2 for mRNA synthesis. Rx3∷nlcam was generated by replacing GFP in pBS-ISceI Rx3∷GFP by the 1.9 -kb nlcam cDNA. Partial clones of *ncam2, ncam3* and *mcam* for *in situ* hybridization probes were amplified from wt cDNA using the following primers:

Ncam2-F: TTCGGCAGGGTGAGGTGGCTGAAGTGGTCT
Ncam2-R: ATTGATTGGCGTGTTCTTGCTTGTATTCTC
Ncam3-F: CGCCATTATCGTGTGTGATGTCATAAGCTC
Ncam3-R: TGATTAGCTGTGGCCTCTTCTTCAGTCCTC
Mcam-F: TGGCGAGAGGGATTTAATAAGCGATGA
Mcam-R: CCTTTGACATTGTTTGAAAGAAAATGCGAG

The products were Topo-cloned into pCRII-TOPO (Invitrogen).

In situ hybridisation

In addition to the amplified cDNAs, the following clones were used to synthesise probes: *alcam* (BC050482); *e-cadherin* (AI629129); *bcam* (CN831659); *integrinβ1b* (BQ075715); *integrinβ4* (BI840449); *integrinβ5* (BC124678); *emx3* (CO959873)—all obtained from ImaGenes (www.imagenes-bio.de). The *n-cadherin* cDNA was given by JD Jontes (Jontes et al., 2004), and subcloned into pBS SK+. The *ncam* cDNA was a gift from D. Grunwald.

Whole mount *in situ* hybridisations were carried out on the progeny of *chk/*+ intercrosses, using Digoxigenin-labelled probes, as described previously (Loosli et al., 1998). Embryos were sectioned by embedding in gelatin/albumen, and 25-μm vibrotome sections were cut.

Rx3 binding site predictions

The mouse RAX consensus binding site previously identified (Berger et al., 2008) was retrieved from the UniPROBE database (Newburger and Bulyk, 2008). Zebrafish *nlcam* and corresponding orthologous genes were retrieved from the EnsEMBL v50 database (Flicek et al., 2008): ENSDARG00000058538 (zebrafish), ENSTRUG00000006355 (fugu), ENSGACG00000010444 (stickleback) and ENSORLG00000005387 (medaka). Occurrences of the RAX position weight matrix were screened in the 20 -kb upstream and intronic sequences of *nlcam* and its orthologues using the POSSUM software (threshold 7) [http://zlab.bu.edu/~mfrith/possum/]. The upstream and intronic RAX binding sites were predicted at the following respective positions from the gene transcription start

site: −12483 → −12467 and 36487 → 36503 (zebrafish), −14076 → −14060 and 9289–9305 (fugu), −18570 → −18554 and 3271 → 3287 (stickleback), −2829 → −2813 and 9344 → 9360 (medaka).

Electrophoretic mobility shift assay (EMSA)

For both predicted Rx3 binding sites, double stranded oligonucleotides were designed to contain the site and flanking regions, plus an additional 5′-GGG overhang for labelling: 5′gggCTGTGCACTTAGCTT-TAATTAGGGGAAAAAAACTTG (upstream), 5′gggAAACTTCTACAGCAT-TAATTAATGCATGTTTTGAGA (intron). Corresponding double stranded oligonucleotides containing a mutated homeobox core binding site were also designed (AATT → CCGG): 5′gggCTGTGCACTTAGCTTT**CCG-G**AGGGGAAAAAAACTTG (Δupstream), 5′gggAAACTTCTACAG-CATT**CCGG**AATGCATGTTTTGAGA (Δintron).

Complementary oligonucleotides were annealed and end-labelled with Klenow DNA polymerase and [α-32P]dCTP. Corresponding cold oligonucleotides were synthesised using non-labelled dCTP for competition assays. Zebrafish Rx3 was *in vitro* translated using the TnT Sp6/T7 coupled reticulocyte lysate system (Promega). 1fmole labelled oligonucleotide was incubated with 5 μl Rx3 translation reaction for 30 min at room temperature in the following binding buffer: KCl 100 mM, MgCl2 10 mM, Hepes (pH 8) 10 mM, DTT 1 mM, Glycerol 5%, EDTA 1 mM and poly(dI:dC) 1 μg, in 20 μl total volume. Competition was performed with 100, 500 or 1000 fold molar excess of cold competitor. The DNA–protein complex was resolved on a native 6% polyacrylamide gel (in 0.5 × TBE) at 160 V at 4 °C for 2 h. The gel was dried and visualised by autoradiography.

Injection and transplantation

Injections were carried out essentially as described [Rembold]. Approximately 10% total cell volume–corresponding to ∼1–1.5 nl–was injected into each embryo at the one-cell stage.

The following mRNAs for injection were synthesised using the mMessage mMachine kit (Ambion): *nlcam* (10–20 ng/μl), *eBFP2-Nuc* (80 ng/μl) (Addgene) (Ai et al., 2007), *H2BmRFP* (80 ng/μl) (Campbell et al., 2002). mRNAs were injected at the concentrations shown. pBS-ISceI Rx3∷GFP and Rx3∷nlcam were injected at 5 ng/μl either alone or in combination.

nlcam morpholinos were obtained from Genetools. The morpholino sequences are as follows:

nlcam-ATG-MO: GCAGTCTGCGATAGTTCTGCACTCC.
nlcam-e3i3-MO: AATGATTCTTACTGTAAATGACCAG.

The *nlcam-ATG-MO* has recently been published (Diekmann and Stuermer, 2009).

Morpholinos were diluted in dH₂O and injected at 0.3 mM (*ATG-MO*) or 0.2 mM (*e3i3-MO*). wt and MO-injected embryos were stage-matched by counting somites.

For transplantation, embryos were dechorionated with Pronase (1 mg/ml in E3 medium) and kept in Balanced Salt Solution. At blastula stages, about 20–50 cells from each donor were transplanted together into the animal pole of stage-matched Rx3∷GFP transgenic host embryos.

Imaging

For calculation of optic vesicle area (Fig. 3G), ImageJ software was used to outline the optic vesicles from images of dorsal views of embryos. The number of pixels within the outlined area was then calculated. Data are shown in arbitrary units, and represents the average area for wt embryos set to 100.

For confocal microscopy, embryos were mounted in 0.8% low melting point agarose in E3 medium, in glass bottomed Petri dishes

(MatTek). Images were obtained on a Leica SP5 confocal with a 20× objective, simultaneously scanning with 405 nm, 488 nm and 561 nm laser lines. z-stacks were recorded every ∼2 min for 8 h, with a voxel size of $1 \times 1 \times 2$ μm. In total, five datasets were recorded. Two were incomplete, as the eye field moved partially out of the field of view during recording. Datasets 1–3 were primarily used for analysis, although the results were confirmed in the incomplete datasets. Although effort was taken to ensure that all datasets covered the same developmental period, there is slight variability (20–30 min) in timing.

Image processing and data analysis

Initially, noise reduction and dye separation algorithms were applied to the confocal stacks, in the Leica LAS AF software. The data were then processed using our digital embryo processing pipeline (Keller et al., 2008), developed in Matlab (The Mathworks). The enhanced segmentation modules allow for automated processing of confocal time-lapse data sets on a single computer workstation. We further extended the data analysis algorithms, as described below.

The segmentation processing pipeline

First, the *x–y*- and *x–z*-projections of the raw image stacks were spatially correlated (subroutine *correlateTL*) to obtain the time-dependent three-dimensional drift vectors and tilt angles. The raw confocal time-lapse datasets were then converted into an image database (subroutine *createID*). Pre-processed information on the experiment was collected and the image stacks were convolved with a three-dimensional Gaussian kernel ($\sigma = 2$ pixels) in order to reduce the noise and to increase the segmentation efficiency. Segmentation of the data was performed with the subroutine *clusterNuclei* as previously described (Keller et al., 2008), using a parallelised multi-core processing scheme on a single workstation.

The segmentation data were analyzed by the spatial- and temporal-domain filters of the processing pipeline (subroutines *clusterFilter* and *clusterCorrelate*). Segmented objects were tested for morphological connectivity, geometrical isotropy of the object surface and consistent spatiotemporal correlation patterns, as previously described (Keller et al., 2008). A final processing module (*clusterSaturate*) facilitated the recovery of false negatives from the initial segmentation database.

The data analysis pipeline

First, migratory tracks within the eye field were determined with the subroutine *clusterTrace*. The eye field masks at four time points (typically time points 50, 100, 150 and 200 in each time-lapse; obtained from the Rx3-eGFP marker) were used as nucleus seeding data sets. Nuclei within the volume defined by each mask were followed forwards and backwards in time by correlating the spatial centre-of-mass coordinates and subsequent tracking of the nuclear identities matching best. Gaps of at maximum one time point were allowed, before the corresponding track was flagged as being discontinued/unknown. In wt/*nlcam*+ experiments, the migratory track of each nucleus had to fulfill the geometrical constraints of at least three checkpoints provided by the Rx3 eye field masks in order to be categorized as belonging to an eye field cell. In wt/*nlcam-MO* experiments, cells within the eye field masks were discarded; converging lateral forebrain cells were then manually selected by virtue of their initial position.

Subsequently, the migratory tracks of wt cells, *nlcam*+ cells and *nlcam*-MO cells were analyzed independently (subroutine *analyzeTable*). The speeds, absolute positions and mean square distances (MSD) were determined for each nucleus as a function of time and separately for each spatial dimension. Time-dependent movement speeds were calculated as slopes of the second-order-polynomial fitting of nucleus positions, using a 20-min sliding window. The MSD at time point *t* was calculated as the squared distance between

nucleus positions at time point *t* and at the start of the recording. Statistical analysis and comparisons were performed for the entire wt, *nlcam*⁺ and *nlcam*-MO cell populations as well as for medial and lateral subgroups (in wt/*nlcam*⁺ experiments). These were defined by measuring the distance from the midline to the most lateral cell, and by dividing the resulting field into two equal-sized groups symmetrically on either side of the midline.

Migration vectors and three-dimensional nucleus distributions were rendered with the custom routines *clusterCombination* and *clusterCones* as a function of time, using POV-Ray (Persistence of Vision Team) as a back-end rendering engine.

All algorithms have been supplied in the Supplementary File "Software Modules."

Results

nlcam is upregulated in rx3/chk mutant embryos

To identify potential CAMs acting downstream of Rx3 in optic vesicle morphogenesis, we searched for genes whose expression was altered in zebrafish *chk* mutants at the 6-somite stage (6SS): when wt and mutant embryos can first be distinguished. Of the 12 genes tested, which included cadherins, integrins and Ig-family CAMs (Table S1 in Supplementary Material and Fig. 1E–L), only *nlcam* showed an obvious misregulation (Figs. 1A, B). In wt embryos, *nlcam* is strongly expressed in a population of dorso-medial cells in the anterior neural tube (Fig. 1A, inset), in addition to weak expression throughout this region. However, in *chk* mutants, the *nlcam* expression domain was expanded ventrally and laterally into the presumptive eye field, which

fails to evaginate (Fig. 1B, inset). This misregulation of *nlcam* was also apparent earlier in development (Figs. 1C, D). In wt bud stage embryos, *nlcam* is expressed at low levels throughout the anterior neural plate, including the eye field (marked by stippled line), but is elevated in a broad stripe at the midline and in the most anterior and lateral cells of the neural plate. These lateral cells are the precursors of the dorsal telencephalon, which migrate medially, ending up in the domain of *nlcam* expression by 6SS (England et al., 2006; Wilson and Houart, 2004). In crosses between *chk* carriers, approximately one quarter of embryos, presumably mutants, showed an expanded *nlcam* domain at the bud stage, with strong expression in the eye field. Double *nlcam, rx3* in situs on *chk*/+ intercrosses demonstrated that those embryos with expanded *nlcam* expression were those with no *rx3* staining (i.e. *chk* mutants) (*n* = 5/22; data not shown).

nlcam is a member of the Alcam subgroup of the Ig-domain superfamily (Swart, 2002). Higher vertebrate genomes encode only a single Alcam molecule (also known as Neurolin, CD166, DM-GRASP and BEN); a teleost-specific duplication event generated the paralogs *neurolin* and *nlcam* (Mann et al., 2006). These molecules participate in homophilic and heterophilic cell–cell adhesion, and have been implicated in a range of developmental processes. Members of the Alcam family are thus attractive candidates for regulating cellular behaviour during morphogenesis.

Rx3 binds predicted motifs in the regulatory regions of nlcam

Given the change in *nlcam* expression upon loss of Rx3, we sought to determine whether *nlcam* might be a direct target of Rx3. To date, there are no confirmed direct targets of this transcription factor and
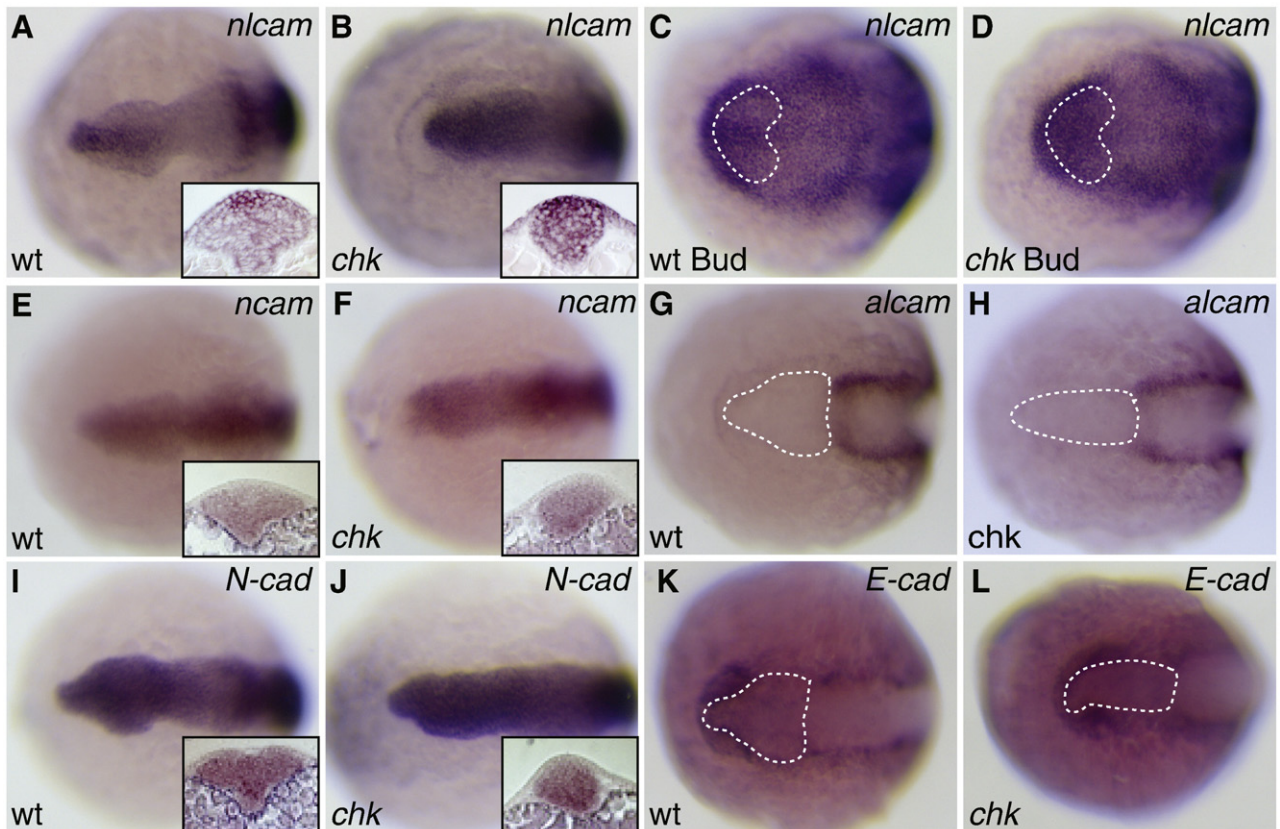
Fig. 1. *nlcam* is specifically upregulated in the *Rx3/chk* mutant. Whole mount *in situ* expression patterns of CAMs in wild type (A, C, E, G, I, K) and *chk* mutant (B, D, F, H, J, L) embryos at the 6S (A, B, E–L) or Bud (C, D) stage. Dorsal views, anterior to the left. (A, B) *nlcam*, 6SS. Insets show cross sections through the anterior neural plate (dorsal is up), showing upregulation of *nlcam* in the *chk* presumptive eye field. (C, D) *nlcam*, Bud stage. *nlcam* is upregulated *in chk* at this stage, shortly after the onset of Rx3 expression (domain marked by white stippled line). No other CAMs tested show changes in expression pattern. E, F: *ncam*. G, H: *alcam*. I, J: *N-cadherin*. K, L: *E-cadherin*. Sections for *ncam* and *N-cadherin*, which are expressed in the eye field, are also shown. For *alcam* and *E-cadherin*, where there is no or very little expression in the eye, the Rx3 expression domain is marked by the white stippled line.

the details of its DNA binding specificity are unknown. However, a mouse Rx (RAX) binding site has recently been identified (Berger et al., 2008). We therefore used this consensus motif to search for potential instances within the upstream and intronic regions of the *nlcam* locus. We identified two potential binding sites for Rx3 in the zebrafish locus, one located approximately 12 kb upstream of the transcription start site, and the other in intron 12 (Fig. 2, upper panels). Predicted sites were also found in other species, suggesting that they could be functional Rx3 binding sites. In order to test for Rx3 binding, we performed electrophoretic mobility shift assays (EMSA) using radioactively-labelled oligonucleotides corresponding to the predicted Rx3 binding site (Fig. 2, lower panels). For both the upstream and intronic motifs, we detected Rx3 binding to the wt oligonucleotides. Addition of increasing concentrations of unlabelled oligonucleotide efficiently competed for Rx3 binding. Additionally, we mutated the central AATT motif to CCGG. These mutant oligonucleotides were not able to bind Rx3, confirming the specificity of the interaction. From these results, we infer that Rx3 can recognise motifs

in the regulatory region of *nlcam*, and therefore that *nlcam* may be a direct target for Rx3. We note that, given the similarity between DNA binding domains Rx3 and its paralogs Rx1 and Rx2, it is also likely that these factors might be able to bind the *nlcam* Rx motif.

nlcam overexpression causes a small eye phenotype

The upregulation of *nlcam* in *chk* mutants suggested that its repression in the eye field is critical for retinal morphogenesis. To test whether ectopic *nlcam* expression disrupts optic vesicle evagination, we ubiquitously overexpressed it by mRNA injection. Embryos injected with 10–20 ng/μl *nlcam* mRNA displayed a range of phenotypes: the majority survived gastrulation, but often displayed a shortened axis, neural tube and somite defects (Figs. 3A–D and Supplementary figure 5A). However, the most prevalent phenotype, seen in approximately 75% of embryos, was a reduction in eye size, either unilaterally (Fig. 3B) or bilaterally (Fig. 3C). Cyclopic embryos were occasionally seen (data not shown), and in the most extreme
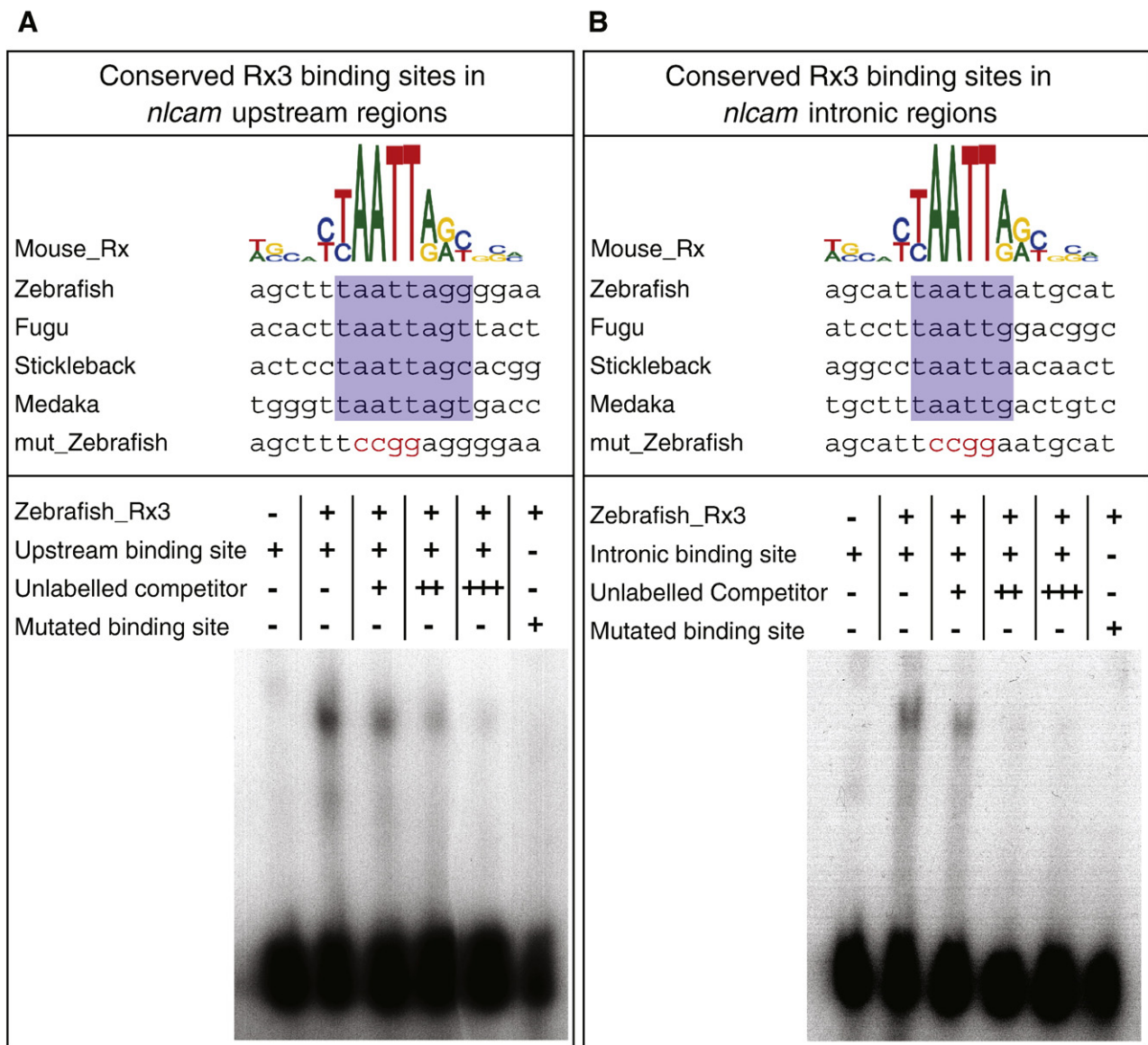
Fig. 2. Electrophoretic mobility shift assays on Rx3 predicted binding sites. Upper panels: in the sequence alignment between the mouse RAX binding site and predicted Rx binding sites the upstream (A) and intronic (B) regions in 4 fish species, conserved nucleotide positions are highlighted in blue. Mutations made within the homeobox core binding site are highlighted in red. Lower panels: Rx3 predicted binding sites in zebrafish *nlcam* were tested by EMSA. Rx3 specifically binds to the oligonucleotides containing the RAX motif, but not to mutated versions. This binding can be competed away by increasing levels of unlabelled oligonucleotide.
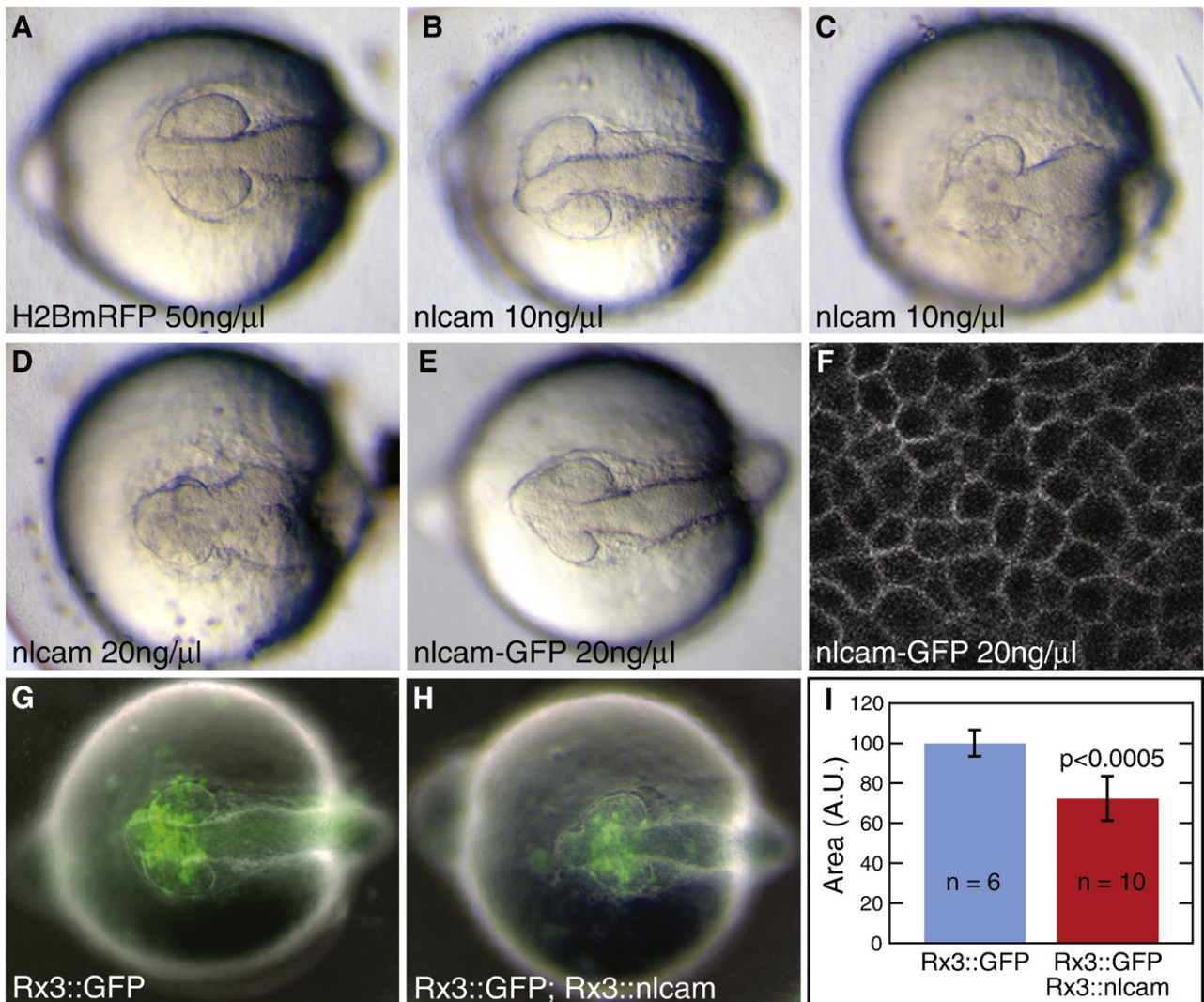
Fig. 3. Overexpression of *nlcam* leads to a reduction in eye size. (A–E) 14SS embryos, injected at the one cell stage with *H2BmRFP* RNA (A), *nlcam* RNA (B–D) or *nlcam-GFP* RNA (E). *nlcam* overexpression leads to a reduction in eye size in a dose-dependent manner. *nlcam-GFP* RNA injection (E) causes a similar range of phenotypes. (F) GFP-tagged Nlcam is localised to the plasma membrane of RPCs. (G, H) 14SS embryos, injected at the one cell stage with Rx3∷GFP (G) or a mixture of Rx3∷GFP and Rx3∷nlcam (H) plasmids. Cells expressing the transgenes are marked by GFP. Overexpression of *nlcam* exclusively in RPCs causes small eyes, while the rest of the embryo is unaffected. (I) Quantification of eye size at 14SS after DNA injection. The area of the optic vesicle, shown in arbitrary units ± standard deviation (set to 100 for the control embryos), is significantly smaller when *nlcam* is overexpressed. n = number of optic vesicles measured.

cases, at higher doses of *nlcam* RNA (Fig. 3D), the eyes were almost absent altogether. Under these conditions, however, the frequency of gastrulation defects was increased. Therefore, in all subsequent experiments, we used the lower 10 ng/μl dose.

To assess the functionality of the *nlcam* cDNA, we injected RNA encoding a C-terminally GFP-tagged *nlcam* into embryos. This led to a similar spectrum of phenotypes (Fig. 3E). By confocal microscopy, we confirmed that Nlcam-GFP was exclusively localised to the plasma membrane in the evaginated optic vesicle (Fig. 3F). This demonstrated that this construct and, by analogy the untagged version, was appropriately localised within the cell and presumably functional.

Thus, ubiquitous *nlcam* overexpression results in a small eye phenotype, similar to hypomorphic, temperature-sensitive medaka *rx3* mutants (Loosli et al., 2001). To further address this, we used the RPC-specific Rx3 promoter (Rembold et al., 2006b) to overexpress *nlcam* in a targeted manner (Rx3∷nlcam). Coinjection of this construct with Rx3∷GFP generated F0 embryos with mosaic expression of *nlcam* in RPCs marked by GFP (Rembold et al., 2006a). We note that some ectopic expression of GFP was observed in non-RPCs; this can be attributed to the leaky nature of transient transgenesis.

Injected embryos displayed reduced eye size relative to Rx3∷GFP injected controls (Fig. 3G–I), but were otherwise normal. We therefore concluded that ectopic expression of *nlcam* in the eye field impaired optic vesicle formation. However, it is notable that GFP-positive cells were dispersed throughout the forebrain and optic vesicle, indicating that migration is not entirely abolished upon overexpression of *nlcam*.

nlcam[+] *cells show abnormal migratory behaviour*

Given the clear reduction in eye size upon *nlcam* overexpression, we followed wt versus *nlcam*-overexpressing (henceforth referred to as *nlcam*^{+}) cells throughout the process of optic vesicle morphogenesis. To do this, we performed "double transplant" experiments (outlined in Fig. 4A). We transplanted cells from two sets of donors, one injected with a mixture of *nlcam* and *H2B-mRFP* RNA and the other with *eBFP2-Nuc* RNA, into the animal pole of Rx3∷GFP hosts. This generated embryos with two populations of transplanted cells: wt cells marked by nuclear eBFP2, and *nlcam*^{+} cells marked by nuclear mRFP. In addition, the eye field was labelled with GFP. Optic
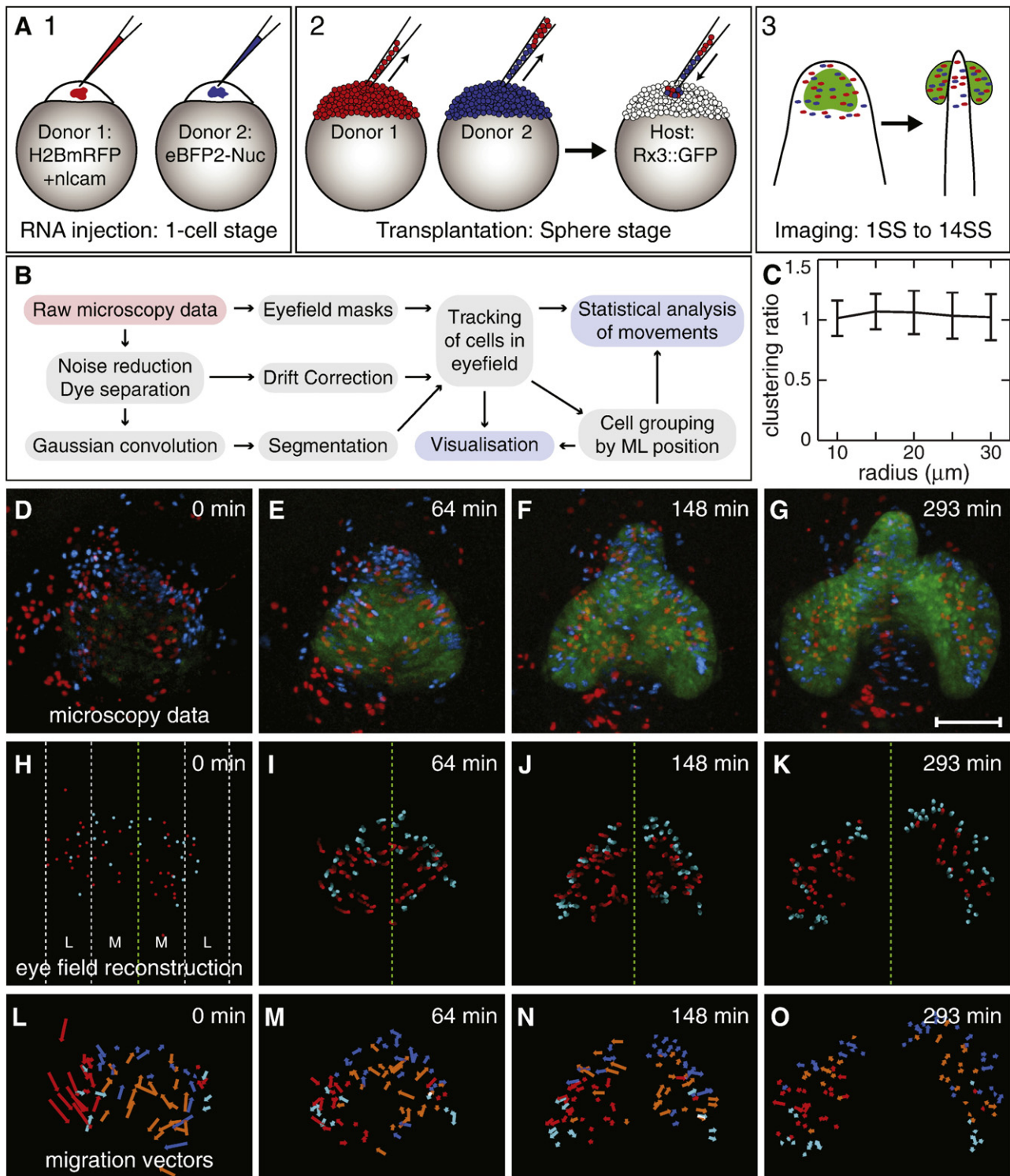
Fig. 4. Analysis of the effects of Nlcam on cell migration during OV morphogenesis. (A) Outline of the experimental procedure. Embryos are injected at the one cell stage with either a mixture of *H2BmRFP* and *nlcam* RNAs or with *eBFP2-Nuc* RNA (1). Cells from both donors are transplanted into Rx3∷GFP hosts (2). After the onset of GFP expression, embryos are imaged by confocal microscopy (3). (B) Outline of the processing pipeline. Red boxes show the input; grey boxes detail the processing steps; and blue boxes show the final output. (C) Clustering analysis of transplanted cells indicates that *nlcam* overexpression does not promote homophilic clustering. (D–G) Selected frames from Dataset 1, showing key points during optic vesicle morphogenesis. Between 0 and 64 min (D, E), RPCs are converging towards the midline. Subsequently, RPCs begin to evaginate (F). Approximately 5 h after the onset of imaging (G), the process is essentially complete. The eye field is marked in green; wt cells are blue; *nlcam*⁺ cells are red. Scale bar is 100 μm. (H-K) Rendered reconstruction of cells within the eye field at the same time points. Trails show the position of the nucleus over the previous 10 time points (~20 min). Green dashed line indicates midline. White dashed lines in H indicate medial (M) and lateral (L) groupings used for analysis. (L–O) Vectorial visualisation of migration. For simplification, the data is collapsed in the DV axis. Arrows show migration direction and displacement of cells over the following 10 time points. Cyan: lateral wt cells. Blue: medial wt cells. Red: lateral *nlcam*⁺ cells. Orange: medial *nlcam*⁺ cells.

vesicle development was then followed by confocal microscopy from soon after the onset of GFP expression (1-2SS, during the convergence stage) for approximately 8 h (14-16SS), by which time the vesicles

were fully evaginated, and the transition to optic cups beginning. In total, five datasets were recorded and analysed; Dataset 1 is shown in Movie 1 in Supplementary Material and selected frames in Fig. 4D–G.

Nuclei were tracked using an enhanced version of our digital embryo processing pipeline (Keller et al., 2008) outlined in Fig. 4B (see Materials and methods for details). This tracked RPCs throughout the time course of optic vesicle evagination, allowing the movements of wt and *nlcam*+ cells to be analysed in detail (Movies S2 and S3 in Supplementary Material, and Figs. 4H–K). Several statistical parameters were extracted from the dataset, including centre-of-mass position, speed and mean square distance (MSD, see Materials and methods for details), all as a function of time. These were also obtained for each of the three axes–medio-lateral (ML), antero-posterior (AP) and dorso-ventral (DV)–independently.

With this digital reconstruction of cell position over time, we first investigated whether *nlcam*+ cells were clustered, as might be expected if Nlcam were mediating homophilic cell adhesion. To this end, we calculated a "clustering score" for both wt and *nlcam*+ cells, at the onset of recording. We define this as the number of nuclei lying within a particular radius from each cell, and normalised to take into account the total number of transplanted cells. From this, we then obtained the "clustering ratio": the ratio of the clustering scores of wt and *nlcam*+ cells, which is a direct measure of the relative degree of clustering of wt and *nlcam*+ populations. A ratio greater than 1 would indicate that *nlcam*+ cells cluster together more than their wt counterparts. However, at all radii tested, the average clustering ratio over seven datasets is approximately 1 (Fig. 4C). This clearly demonstrates that *nlcam*+ do not cluster, arguing strongly against the idea that Nlcam is participating in homophilic cell adhesion in this context.

Next, we analysed the dynamics of wt and *nlcam*+ cell migration. In the wild-type situation, similar to what has been observed in medaka (Rembold et al., 2006b), laterally located cells migrate more rapidly and further towards the midline that medially located cells. Subsequently, these initially laterally located cells then migrate outwards more rapidly as well (compare graphs for wt cells in Fig. 5
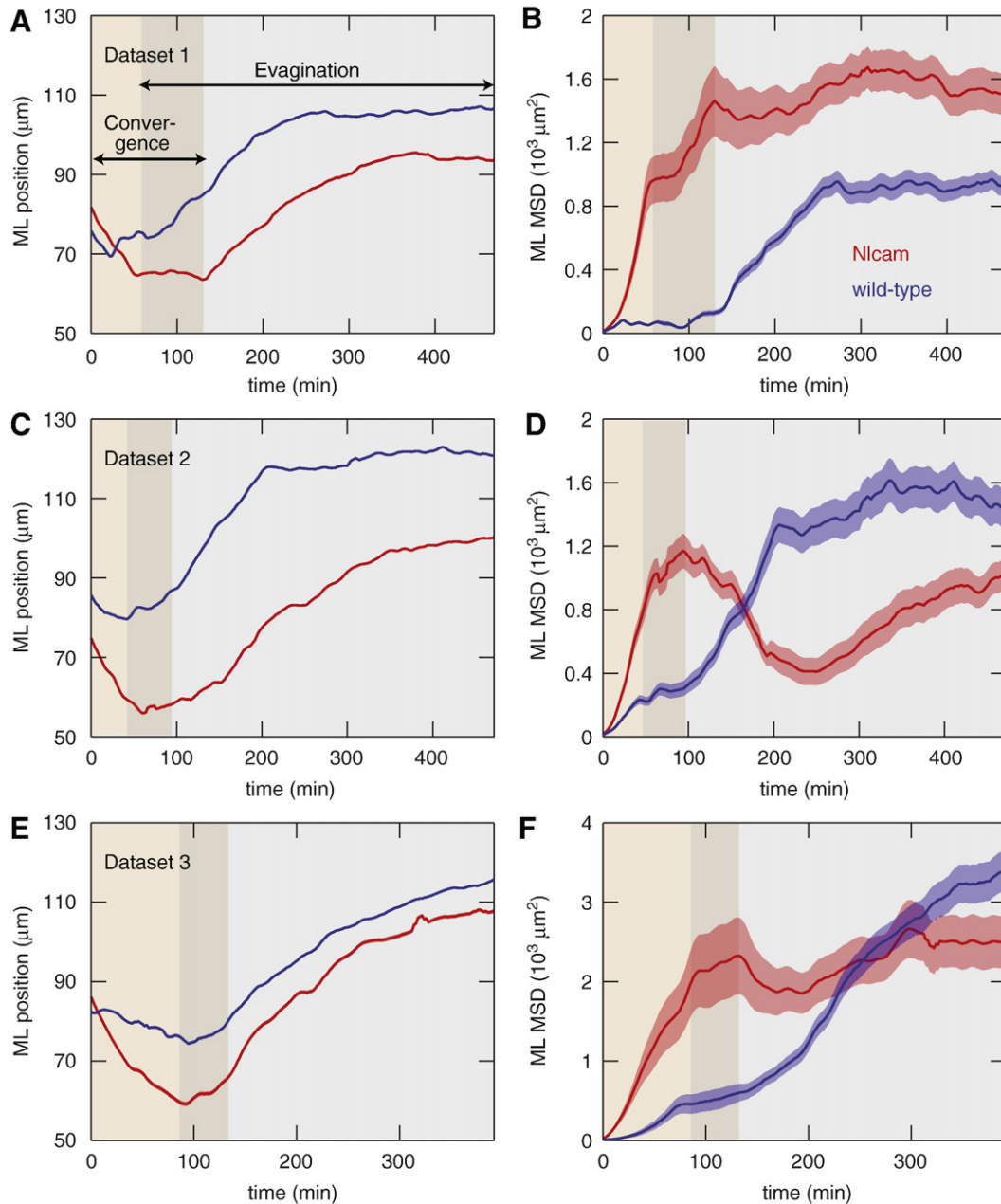
Fig. 5. Statistical analysis of migratory dynamics of lateral retinal cells. Graphs show selected statistics for the lateral groups of cells from datasets 1–3. (A, C, E) Position of cells relative to the midline. (B, D, F) MSD along the ML axis. Blue: wt cells. Red: *nlcam*+ cells. Paler shading indicates standard error. Overlapping boxes show the approximate periods of convergence (brown) and evagination (grey).

and Supplementary Figure 2). Given the complicated movements occurring here, statistical analysis of RPC migration would be obscured by considering all cells together (Fig. S1 in Supplementary Material). To improve the resolution of our analysis, the tracked cells were divided into two groups according to their initial medio-lateral position (Fig. 4H). We then determined the statistics for each group ("medial" and "lateral") separately. The behaviour of wt cells closely resembled the situation in medaka (Rembold et al., 2006a), demonstrating that the mechanism of optic vesicle evagination is conserved among teleosts.

The grouped statistics revealed striking differences in behaviour of lateral wt and *nlcam*$^+$ cells in the ML axis (Fig. 5). In all datasets, laterally located *nlcam*$^+$ cells converged further towards the midline (Figs. 5A, C, E) than did equivalent wt cells. They then migrated outwards at a similar rate to the wt population, and thus remained more medially positioned as the vesicles evaginated. This resulted in a final distribution where the lateral-most domains of the optic vesicles were primarily populated by wt cells, whereas *nlcam*$^+$ cells tended to occupy more medial positions (Fig. 4G). These positional biases are reinforced by differences in the dynamics of migration revealed by the ML MSD plots (Figs. 5B, D, F). Wt cells accumulated most of their MSD during the outward-directed phase of migration, whereas *nlcam*$^+$ cells accumulated much more during convergence, and reached at least 50% of their final MSD within the first hour of recording (Supplementary Table 2). In contrast to the consistent differences in behaviour between the lateral populations, the medial groups did not show an obvious differential phenotype (Fig. S2 in Supplementary Material).

To visualise the differences in behaviour more clearly, we generated movies in which the displacement of each cell over 20 min is shown by an arrow: longer arrows thus indicate greater movement (Movie 4 in Supplementary Material, and Figs. 4L–O). During the initial phase of recording, the lateral *nlcam*$^+$ cells (red arrows) displaced much further than the wt cells (cyan arrows) (Fig. 4L). At later time points, no obvious differences could be observed between wt and *nlcam*$^+$ cells,

with both populations migrating outwards into the growing optic vesicles (Figs. 4M–O).

We next considered whether biased distribution of the *nlcam*$^+$ versus wt cells in the other axes might contribute to the differences in behaviour. There was no consistent bias in the AP axis (Fig. S3A, C, E in Supplementary Material). However, in all three datasets, lateral *nlcam*$^+$ cells were more dorsally located than wt cells at the onset of recording (see anterior and lateral views of Movie 3 and Fig. S3B, D, F in Supplementary Material, and Supplementary Table 2), suggesting that Nlcam may affect the DV position of RPCs. To test for possible DV effects on RPC migration, we split the lateral wt population into dorsal and ventral groups and compared these. Similar to medaka (Rembold et al., 2006a), dorsal wt cells converged further towards the midline than ventral cells (Fig. S4A, C, E in Supplementary Material). However, the migratory dynamics of the dorso-lateral wt cells was very different from that of the lateral *nlcam*$^+$ population (Fig. S4B, D, F; Supplementary Table 2). We therefore concluded that, while DV position does affect RPC migration, it is the overexpression of *nlcam* that is primarily responsible for the enhanced midline convergence of these cells.

The phenotype of *nlcam*$^+$ cells was reminiscent of the rapid midline-directed migration of lateral telencephalic cells. To further investigate this similarity, we tracked selected wt forebrain cells by manually picking cells that originated lateral to the eye field and remained at the midline after convergence (yellow cells in Movie 2 in Supplementary Material). The initial rate of MSD accumulation of these cells was very similar to that of the lateral *nlcam*$^+$ group (Supplementary Table 2). Subsequently, however, these two populations diverged as the *nlcam*$^+$ RPCs underwent evagination while the telencephalic cells continued to migrate medially.

Defective forebrain cell convergence upon nlcam knock-down

Given that *nlcam* is normally expressed in lateral forebrain precursors, we wondered whether the phenotype we observed
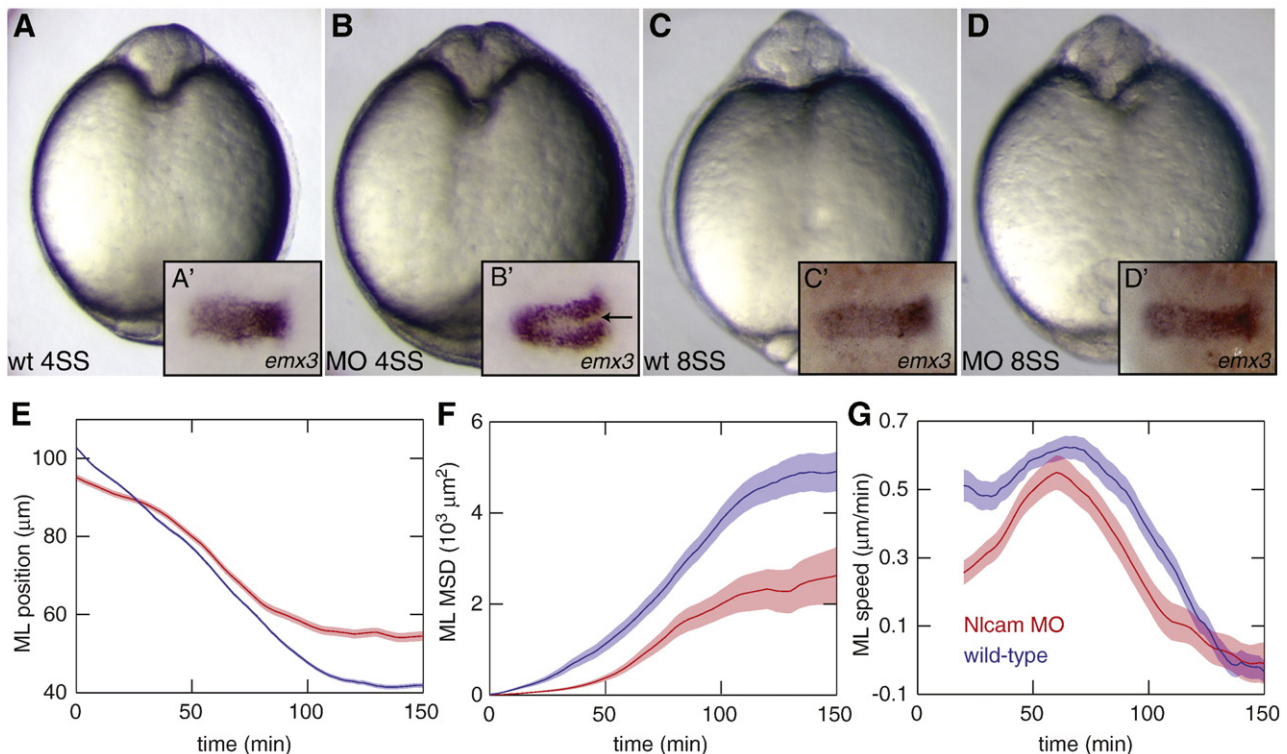
Fig. 6. *nlcam* loss of function causes delayed convergence. (A–D) At 4SS, a deep cleft at the midline in *nlcam ATG-MO* injected (0.3 mM) embryos (B) indicates that forebrain cells have not yet converged to the midline, as they have in control embryos (A). This is confirmed by *in situ* hybridisation against *emx3* (A′, B′). This phenotype is transient, as demonstrated by the recovered forebrain morphology by 8SS (C, D). (E–G) Graphs show selected statistics for forebrain cell convergence from a single dataset. (E) Position of cells relative to the midline. (F) MSD along the ML axis. (G) Speed along the ML axis. Blue = wt cells; red = *nlcam-MO*.

upon ectopic *nlcam* overexpression in RPCs might reflect an endogenous function in promoting convergence in these forebrain cells. To test this, we designed a morpholino to block translation of *nlcam* (*nlcam ATG-MO*) and injected this into embryos. The efficacy of *nlcam ATG-MO* was confirmed using an RNA in which the target sequence was placed upstream of GFP. Coinjection of this RNA and *nlcam ATG-MO* at 0.3 mM led to an almost complete abrogation of GFP expression (Supplementary Figure 5C, D). Analysis of morphant embryos revealed a transient phenotype: at 4SS, a deep cleft was visible at the anterior midline of *nlcam ATG-MO* injected embryos, but not control embryos (Figs. 6A, B). However, by 8SS, this phenotype had almost completely recovered (Figs. 6C, D) in the majority of embryos. This delayed convergence of forebrain precursors was also validated by *in situ* hybridisation against the early forebrain marker *emx3*. In wt embryos at 4SS, *emx3* was detected as a broad domain at the midline (Fig. 6A′). In somite-matched *nlcam ATG-MO* injected embryos, however, the two *emx3* stripes had not completely converged, leaving a gap at the midline (Fig. 6B′). As expected, cells ventral and medial to the *emx3* stripes express the eye field marker Rx3 (data not shown). Similar results were obtained with a second morpholino, directed against the exon3–intron3 splice junction, confirming the specificity of the phenotype (Supplementary Figure 5F).

To further confirm this delayed convergence phenotype, we again performed double transplant and live imaging experiments. In this case, donor embryos were either injected with a mixture of *H2B-mRFP* RNA and *nlcam ATG-MO* or with *eBFP2-Nuc* RNA. Cells from both donors were transplanted into Rx3∷GFP hosts, and imaged as before. Following segmentation, cells lying lateral to the Rx3∷GFP positive eye field were tracked. Statistical analysis of these movements confirmed the observed defect in forebrain convergence: *nlcam ATG-MO* cells moved more slowly towards the midline (Figs. 6E, G), and did not accumulate as much MSD (Fig. 6F) during the initial phase of convergence. In combination, these results indicated that loss of *nlcam* function led to a slowed convergence of lateral forebrain cells, although the later recovery of the phenotype

suggests that they are able to reach their final position, albeit with slower kinetics.

Discussion

Understanding how Rx3 controls eye morphogenesis requires the identification of downstream factors that regulate cellular morphogenetic behaviours. Here, we have identified one such player: the Ig-domain CAM Nlcam. Uncovering the highly specific effect of Nlcam on RPCs during convergence was only possible by combining advanced experimental embryology and 4D microscopy at high spatio-temporal resolution with a powerful automated image processing and data analysis pipeline that facilitates the tracking of hundreds of cells throughout optic vesicle morphogenesis. Comprehensive reconstructions of the tracks obtained simultaneously in multiple embryos revealed stereotyped, differential migratory behaviours of wt and *nlcam⁺* cells.

Our results are summarised in Fig. 7. Under wt conditions, the action of Rx3 ensures that *nlcam* levels are kept low in the eye field, while it is strongly expressed in the laterally located telencephalic precursors. Although we have not showed definitively that Rx3 directly represses *nlcam* expression, our binding assays show that Rx3 can bind to *nlcam* regulatory sequences (at least in vitro), and we therefore suggest that, *in vivo* the regulation of *nlcam* by Rx3 may be a direct repression. Under our experimental conditions, upon ectopic *nlcam* expression, lateral RPCs took on some of the migratory characteristics of their telencephalic neighbours: they showed highly directed migration towards the midline, and converged further than their wt retinal counterparts. Although they were able to evaginate (demonstrating that there was no change in cell fate), the net result of the aberrant inwards migration was that *nlcam⁺* cells occupied more medial positions in the optic vesicles.

These results have two important implications. Firstly, they provide part of the explanation as to how Rx3 controls retinal morphogenesis. To allow slowed midline convergence of RPCs, Rx3
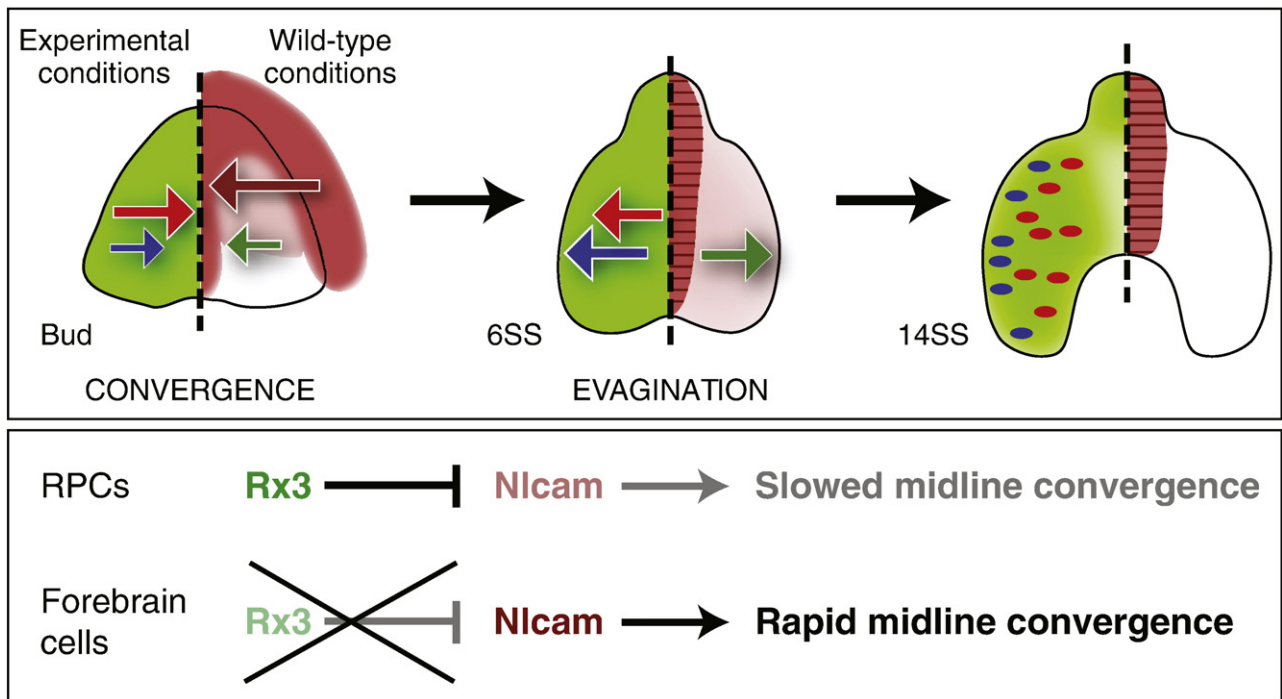
Fig. 7. Summary of effects of Nlcam on cell behaviour. Upper panel: left side indicates the migration of wt (blue) and *nlcam⁺* (red) transplanted cells during optic vesicle morphogenesis. Arrow length indicates the degree of migration. The differential behaviours result in a final distribution where *nlcam⁺* cells occupy more medial positions in the evaginated vesicles. Right side represents the endogenous expression pattern of *nlcam* (maroon), and the normal movements of forebrain and retinal (green) cells. Telencephalic cells, expressing high levels of *nlcam*, migrate rapidly inwards and then epithelialise to form the neural keel. RPCs, with low *nlcam* levels, converge less and then migrate outwards into the optic vesicles. Lower panel: summary of the effects of Rx3 on Nlcam expression and hence on midline convergence of RPCs and forebrain cells.

must downregulate *nlcam* expression within the eye field. Otherwise, the ectopic Nlcam will cause lateral retinal cells converge too far, resulting in reduced optic vesicle size. Secondly, our analysis suggests that one important difference, in morphogenetic terms, between the eye field and the lateral telencephalic domain is the expression level of *nlcam*. This proposal is borne out by our loss-of-function analysis. When Nlcam expression was inhibited by morpholino injection, forebrain cells exhibit slowed convergence to the midline. We therefore propose that Nlcam is a driving force for the rapid medial-directed migration of forebrain precursors.

Alcam family members act through both homophilic and heterophilic interactions, raising the question as to how Nlcam might mediate differences in migratory dynamics. Our analysis indicated that *nlcam* does not promote clustering of transplanted cells, demonstrating that Nlcam does not mediate homophilic cell interactions during neural plate convergence. Beyond homophilic adhesion, there is considerable evidence for a broader function for the Alcam family, both during development and in cancer progression. Alcam has been implicated in axonal pathfinding: in both fish and chick, guidance defects in retinal ganglion cells and motor axons have been observed upon Alcam inhibition (Avci et al., 2004; Ott et al., 1998, 2001). A recent study has shown that Alcam is required for retinal ganglion cell survival, and for survival of other neurons in the retina, and also implicated Nlcam in retinal ganglion cell axon guidance (Diekmann and Stuermer, 2009). Alcam function is also required for non-radial cell migration in the chick diencephalon (Heffron and Golden, 2000). Furthermore, the apparently counter-intuitive observation that Alcam expression correlates with metastatic potential of melanomas and other cancers (Swart et al., 2005) suggests more complex roles for Alcam. This has been borne out by evidence implicating Alcam in ECM remodelling (Lunter et al., 2005) and in intercellular signalling (Ibáñez et al., 2006). Through detailed statistical analysis of cell migration during anterior neural plate morphogenesis, we provide an *in vivo* system in which Nlcam function can be dissected.

Our results suggest a model whereby Nlcam, acting via heterophilic interactions, forms part of the guidance system for morphogenesis of the anterior neural plate. Midline guidance signals have been postulated to account for the migratory behaviour of retinal and forebrain cells (Rembold et al., 2006b). According to this model, telencephalic cells respond strongly to the signals directing midline migration, thus converging rapidly. RPCs, however, respond only weakly, creating a wide eye domain. Subsequent outward directed migration of RPCs might be controlled either by repellent cues from the midline, or by attractive ones from lateral cells. Forebrain precursors would not respond to this set of cues, and instead remain at the midline and epithelialise. We propose that Nlcam may be part of the mechanism responsible for sensing the initial guidance cue: high *nlcam* levels allow forebrain precursors to sense the attractant more acutely than RPCs. Loss of *nlcam* in forebrain cells would therefore result in an attenuated response, and slowed midline convergence. Conversely, when *nlcam* is ectopically expressed in lateral RPCs, they would respond more strongly to the proposed attractant, resulting in their rapid inward migration. Although this model is speculative, it provides a framework for future study. One clear conclusion that can be drawn from our analysis is that the processes of convergence and evagination are genetically separable: Nlcam affects only the former, while other factors downstream of Rx3 must control the subsequent outward-directed migration.

Our sophisticated *in vivo* analysis of the morphogenetic movements in the entire anterior neural plate region has revealed a critical role for Nlcam in modulating the convergence behaviour of differentially specified cell types. Presumably, multiple such effectors must be required to implement the full morphogenetic activity transcriptionally controlled by Rx3. Here, we have identified the first of these molecules; the future challenge is to identify further effectors and to uncover their particular role in the morphogenesis of the vertebrate eye.

Appendix A. Supplementary data

Supplementary data associated with this article can be found, in the online version, at doi:10.1016/j.ydbio.2009.12.003.

References

Adler, R., Canto-Soler, M.V., 2007. Molecular mechanisms of optic vesicle development: complexities, ambiguities and controversies. Dev. Biol. 305, 1–13.

Ai, H.W., Shaner, N.C., Cheng, Z., Tsien, R.Y., Campbell, R.E., 2007. Exploration of new chromophore structures leads to the identification of improved blue fluorescent proteins. Biochemistry 46, 5904–5910.

Andreazzoli, M., Gestri, G., Angeloni, D., Menna, E., Barsacchi, G., 1999. Role of Xrx1 in Xenopus eye and anterior brain development. Development 126, 2451–2460.

Andreazzoli, M., Gestri, G., Cremisi, F., Casarosa, S., Dawid, I.B., Barsacchi, G., 2003. Xrx1 controls proliferation and neurogenesis in Xenopus anterior neural plate. Development 130, 5143–5154.

Avci, H.X., Zelina, P., Thelen, K., Pollerberg, G.E., 2004. Role of cell adhesion molecule DM-GRASP in growth and orientation of retinal ganglion cell axons. Dev. Biol. 271, 291–305.

Berger, M.F., Badis, G., Gehrke, A.R., Talukder, S., Philippakis, A.A., Pena-Castillo, L., Alleyne, T.M., Mnaimneh, S., Botvinnik, O.B., Chan, E.T., Khalid, F., Zhang, W., Newburger, D., Jaeger, S.A., Morris, Q.D., Bulyk, M.L., Hughes, T.R., 2008. Variation in homeodomain DNA binding revealed by high-resolution analysis of sequence preferences. Cell 133, 1266–1276.

Bokel, C., Brown, N.H., 2002. Integrins in development: moving on, responding to, and sticking to the extracellular matrix. Dev. Cell 3, 311–321.

Campbell, R.E., Tour, O., Palmer, A.E., Steinbach, P.A., Baird, G.S., Zacharias, D.A., Tsien, R.Y., 2002. A monomeric red fluorescent protein. Proc. Natl. Acad. Sci. U. S. A. 99, 7877–7882.

Cavodeassi, F., Carreira-Barbosa, F., Young, R.M., Concha, M.L., Allende, M.L., Houart, C., Tada, M., Wilson, S.W., 2005. Early stages of zebrafish eye formation require the coordinated activity of Wnt11, Fz5, and the Wnt/beta-catenin pathway. Neuron 47, 43–56.

Chow, R.L., Lang, R.A., 2001. Early eye development in vertebrates. Annu. Rev. Cell. Dev. Biol. 17, 255–296.

Chuang, J.C., Raymond, P.A., 2001. Zebrafish genes rx1 and rx2 help define the region of forebrain that gives rise to retina. Dev. Biol. 231, 13–30.

Diekmann, H., Stuermer, C.A., 2009. Zebrafish neurolin-a and -b, orthologs of ALCAM, are involved in retinal ganglion cell differentiation and retinal axon pathfinding. J. Comp. Neurol. 513, 38–50.

England, S.J., Blanchard, G.B., Mahadevan, L., Adams, R.J., 2006. A dynamic fate map of the forebrain shows how vertebrate eyes form and explains two causes of cyclopia. Development 133, 4613–4617.

Flicek, P., Aken, B.L., Beal, K., Ballester, B., Caccamo, M., Chen, Y., Clarke, L., Coates, G., Cunningham, F., Cutts, T., Down, T., Dyer, S.C., Eyre, T., Fitzgerald, S., Fernandez-Banet, J., Graf, S., Haider, S., Hammond, M., Holland, R., Howe, K.L., Howe, K., Johnson, N., Jenkinson, A., Kahari, A., Keefe, D., Kokocinski, F., Kulesha, E., Lawson, D., Longden, I., Megy, K., Meidl, P., Overduin, B., Parker, A., Pritchard, B., Prlic, A., Rice, S., Rios, D., Schuster, M., Sealy, I., Slater, G., Smedley, D., Spudich, G., Trevanion, S., Vilella, A.J., Vogel, J., White, S., Wood, M., Birney, E., Cox, T., Curwen, V., Durbin, R., Fernandez-Suarez, X.M., Herrero, J., Hubbard, T.J., Kasprzyk, A., Proctor, G., Smith, J., Ureta-Vidal, A., Searle, S., 2008. Ensemble 2008. Nucleic Acids Res. 36, D707–D714.

Geiger, B., Bershadsky, A., Pankov, R., Yamada, K.M., 2001. Transmembrane crosstalk between the extracellular matrix–cytoskeleton crosstalk. Nat. Rev. Mol. Cell. Biol. 2, 793–805.

Halbleib, J.M., Nelson, W.J., 2006. Cadherins in development: cell adhesion, sorting, and tissue morphogenesis. Genes Dev. 20, 3199–3214.

Heffron, D.S., Golden, J.A., 2000. DM-GRASP is necessary for nonradial cell migration during chick diencephalic development. J. Neurosci. 20, 2287–2294.

Ibáñez, A., Sarrias, M.R., Farnós, M., Gimferrer, I., Serra-Pagès, C., Vives, J., Lozano, F., 2006. Mitogen-activated protein kinase pathway activation by the CD6 lymphocyte surface receptor. J. Immunol. 177, 1152–1159.

Jontes, J.D., Emond, M.R., Smith, S.J., 2004. In vivo trafficking and targeting of N-cadherin to nascent presynaptic terminals. J. Neurosci. 24, 9027–9034.

Keller, P.J., Schmidt, A.D., Wittbrodt, J., Stelzer, E.H., 2008. Reconstruction of zebrafish early embryonic development by scanned light sheet microscopy. Science 322, 1065–1069.

Kennedy, B.N., Stearns, G.W., Smyth, V.A., Ramamurthy, V., van Eeden, F., Ankoudinova, I., Raible, D., Hurley, J.B., Brockerhoff, S.E., 2004. Zebrafish rx3 and mab21l2 are required during eye morphogenesis. Dev. Biol. 270, 336–349.

Kenyon, K.L., Zaghloul, N., Moody, S.A., 2001. Transcription factors of the anterior neural plate alter cell movements of epidermal progenitors to specify a retinal fate. Dev. Biol. 240, 77–91.

Li, Z., Joseph, N.M., Easter Jr., S.S., 2000. The morphogenesis of the zebrafish eye, including a fate map of the optic vesicle. Dev. Dyn. 218, 175–188.

Loosli, F., Köster, R.W., Carl, M., Krone, A., Wittbrodt, J., 1998. Six3, a medaka homologue of the Drosophila homeobox gene sine oculis is expressed in the anterior embryonic shield and the developing eye. Mech. Dev. 74, 159–164.

Loosli, F., Winkler, S., Burgtorf, C., Wurmbach, E., Ansorge, W., Henrich, T., Grabher, C., Arendt, D., Carl, M., Krone, A., Grzebisz, E., Wittbrodt, J., 2001. Medaka eyeless is the key factor linking retinal determination and eye growth. Development 128, 4035–4044.

Loosli, F., Staub, W., Finger-Baier, K.C., Ober, E.A., Verkade, H., Wittbrodt, J., Baier, H., 2003. Loss of eyes in zebrafish caused by mutation of chokh/rx3. EMBO Rep. 4, 894–899.

Lunter, P.C., van Kilsdonk, J.W., van Beek, H., Cornelissen, I.M., Bergers, M., Willems, P.H., van Muijen, G.N., Swart, G.W., 2005. Activated leukocyte cell adhesion molecule (ALCAM/CD166/MEMD), a novel actor in invasive growth, controls matrix metalloproteinase activity. Cancer Res. 65, 8801–8808.

Mann, C., Hinits, Y., Hughes, S., 2006. Comparison of neurolin (ALCAM) and neurolin-like cell adhesion molecule (NLCAM) expression in zebrafish. Gene Expression Patterns.

Mathers, P., Grinberg, A., Mahon, K., Jamrich, M., 1997. The Rx homeobox gene is essential for vertebrate eye development. Nature 387, 603–607.

Medina-Martinez, O., Amaya-Manzanares, F., Liu, C., Mendoza, M., Shah, R., Zhang, L., Behringer, R.R., Mahon, K.A., Jamrich, M., 2009. Cell-autonomous requirement for rx function in the mammalian retina and posterior pituitary. PLoS One 4, e4513.

Moore, K.B., Mood, K., Daar, I.O., Moody, S.A., 2004. Morphogenetic movements underlying eye field formation require interactions between the FGF and ephrinB1 signaling pathways. Dev. Cell. 6, 55–67.

Newburger, D.E., Bulyk, M.L., 2008. UniPROBE: an online database of protein binding microarray data on protein-DNA interactions. Nucleic Acids Res.

Ott, H., Bastmeyer, M., Stuermer, C.A., 1998. Neurolin, the goldfish homolog of DM-GRASP, is involved in retinal axon pathfinding to the optic disk. J. Neurosci. 18, 3363–3372.

Ott, H., Diekmann, H., Stuermer, C.A., Bastmeyer, M., 2001. Function of Neurolin (DM-GRASP/SC-1) in guidance of motor axons during zebrafish development. Dev. Biol. 235, 86–97.

Rembold, M., Lahiri, K., Foulkes, N.S., Wittbrodt, J., 2006a. Transgenesis in fish: efficient selection of transgenic fish by co-injection with a fluorescent reporter construct. Nat. Protoc. 1, 1133–1139.

Rembold, M., Loosli, F., Adams, R.J., Wittbrodt, J., 2006b. Individual cell migration serves as the driving force for optic vesicle evagination. Science 313, 1130–1134.

Rojas-Munoz, A., Dahm, R., Nusslein-Volhard, C., 2005. chokh/rx3 specifies the retinal pigment epithelium fate independently of eye morphogenesis. Dev. Biol. 288, 348–362.

Rougon, G., Hobert, O., 2003. New insights into the diversity and function of neuronal immunoglobulin superfamily molecules. Annu. Rev. Neurosci. 26, 207–238.

Schmitt, E., Dowling, J., 1994. Early Eye morphogenesis in the Zebrafish, Brachydanio rerio. Journal of Comparative Neurology 344, 532–542.

Stigloher, C., Ninkovic, J., Laplante, M., Geling, A., Tannhäuser, B., Topp, S., Kikuta, H., Becker, T.S., Houart, C., Bally-Cuif, L., 2006. Segregation of telencephalic and eye-field identities inside the zebrafish forebrain territory is controlled by Rx3. Development 133, 2925–2935.

Swart, G.W., 2002. Activated leukocyte cell adhesion molecule (CD166/ALCAM): developmental and mechanistic aspects of cell clustering and cell migration. Eur. J. Cell. Biol. 81, 313–321.

Swart, G.W., Lunter, P.C., Kilsdonk, J.W., Kempen, L.C., 2005. Activated leukocyte cell adhesion molecule (ALCAM/CD166): signaling at the divide of melanoma cell clustering and cell migration? Cancer Metastasis Rev. 24, 223–236.

Tepass, U., Truong, K., Godt, D., Ikura, M., Peifer, M., 2000. Cadherins in embryonic and neural morphogenesis. Nat. Rev. Mol. Cell. Biol. 1, 91–100.

Voronina, V.A., Kozhemyakina, E.A., O'Kernick, C.M., Kahn, N.D., Wenger, S.L., Linberg, J.V., Schneider, A.S., Mathers, P.H., 2004. Mutations in the human RAX homeobox gene in a patient with anophthalmia and sclerocornea. Hum. Mol. Genet. 13, 315–322.

Wilson, S.W., Houart, C., 2004. Early steps in the development of the forebrain. Dev. Cell. 6, 167–181.

Winkler, S., Loosli, F., Henrich, T., Wakamatsu, Y., Wittbrodt, J., 2000. The conditional medaka mutation eyeless uncouples patterning and morphogenesis of the eye. Development 127, 1911–1919.

Woo, K., Fraser, S.E., 1995. Order and coherence in the fate map of the zebrafish nervous system. Development 121, 2595–2609.

Zaghloul, N.A., Moody, S.A., 2007. Alterations of rx1 and pax6 expression levels at neural plate stages differentially affect the production of retinal cell types and maintenance of retinal stem cell qualities. Dev. Biol. 306, 222–240.

Zhang, L., Mathers, P.H., Jamrich, M., 2000. Function of Rx, but not Pax6, is essential for the formation of retinal progenitor cells in mice. Genesis 28, 135–142.